ISBN: 978-3-95450-249-3 ISSN: 2673-5350 doi: 10.18429/JACoW-IBIC2024-WEP30

DETAILED BENCH INVESTIGATIONS AND COMPARISON OF FOUR LOW-LIGHT CAMERAS

L. Bauer*[1], P. Forck[1], S. Udrea
GSI Helmholtzzentrum für Schwerionenforschung GmbH, Darmstadt, Germany
[1]also at Goethe-Universität, Frankfurt am Main, Germany

Abstract

We compared four low-light cameras based on different principles: an Image Intensifier equipped with a double MCP and relay-coupled to an off-the-shelf CMOS camera, an electron-multiplied CCD, and two different sCMOS cameras. LEDs generate light pulses with wavelengths in the range of 385 to 500 nm and a duration of 0.05 to 8 ms to vary the fluence at the camera sensors. Moreover, the spatial resolution is compared. Depending on the wavelength, the Image Intensifier and EMCCD have comparable sensitivity for pulse duration larger than 0.5 ms. However, the spatial resolution of the EMCCD is higher. The sCMOS cameras provide a factor of 5 to 10 lower sensitivity.

INTRODUCTION

Low-light cameras are frequently deployed in beam instrumentation for cases such as low beam current, small beam-induced photon yield or low detection probability. Examples are profile determinations by Beam Induced Fluorescence (BIF) monitors as used at GSI and CERN [1–4], scintillation screens for low beam currents or Optical Transition Radiation (OTR) for low beam velocities [5–7]. In several of the cited applications, cameras with attached Image Intensifiers (hereafter called ICCD) are used. The intensifiers comprise a photo-cathode, a Micro-Channel Plate (MCP) for photo-electron amplification and a phosphor screen. As an alternative, an electron-multiplication CCD camera (EMCCD) was tested, see, e.g. [8, 9]. The working principle of such cameras is based on a CCD sensor and the amplification of the low amount of photo-electrons by a chain of avalanche diodes.

Direct comparisons of low-light cameras for the typical parameters in beam instrumentation are rarely reported, with the exception of Ref. [10]. In the actual contribution, we compare an Image Intensifier and an EMCCD camera operational at GSI to the recently available sensitive scientific CMOS camera type from two manufacturers. Those sCMOS cameras are operated without any electron multiplication stage; instead, the analogue stages and ADC conversion are optimized for low noise. A dedicated test bench was realized to determine the photon sensitivity and any noise contributions under reproducible low-light test conditions. As a light source we used pulsed LEDs to vary the fluence independently of the background, and simulate the beam properties at pulsed ion Linacs or transfer between synchrotrons.

* l.bauer@physik.uni-frankfurt.de

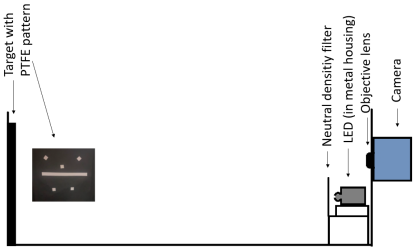

Figure 1: Schematic of the inside of the dark enclosure.

LIGHT SOURCE CHARACTERIZATION

Pulsed LEDs with nominal wavelengths in the range from 385 to 500 nm were used as light sources. Each LED was characterized by an optical spectrometer and photodiode timing measurements. It is ensured that each LED has its emission peak at a wavelength within the expected tolerances, emits in a reasonably narrow wavelength range of 4 to 13 nm (one standard deviation), and that the light pulses follow the electrical driving pulses. The individual LED characteristics are compiled in [11].

The measurements for characterizing the cameras were performed with light pulses between 0.5 and 8 ms. For the ICCD, additional measurements with a light pulse of 0.05 ms were performed. The leading edges of each light pulse was set to 0.1 µs and its trailing edge to 1 µs.

EXPERIMENTAL SET-UP AND CAMERAS

The experimental set-up for camera characterization contains in addition to the light source, a dark enclosure, a function generator (AFG 3102, Tektronix), an oscilloscope (DPO 3034, Tektronix) and a laptop to run the respective camera control software. The cameras are mounted at a wall of the dark enclosure with only the objective lens inside it. The same objective lens (FL-CC1614-2M, RICOH) with a focal length of 16 mm was used for all cameras.

Inside the dark enclosure, at a distance of 87 ± 0.5 cm to the objective lens, a target containing a pattern made of porous, sintered PTFE (PMR10, Thorlabs) is mounted. As shown in Fig. 1, the LED is installed in a dedicated housing and placed below the objective lens in front of a neutral density filter (UVFS Reflective ND Filter, Thorlabs). All non-reflective surfaces inside the dark enclosure are coated with blackened aluminium foil (BKF12, Thorlabs), with a reflectance below 5 % in the relevant wavelength range.

The ProEM:+512B (Teledyne Princeton Instruments [12]) EMCCD camera was used with different electron multiplication gains in the full frame mode. In this contribution,

ISBN: 978-3-95450-249-3 ISSN: 2673-5350 doi: 10.18429/JACoW-IBIC2024-WEP30

we show the results for a gain of 100, the maximum recommended by the manufacturer. The CCD sensor's quantum efficiency peaks at a wavelength of ≃ 600 nm and achieves almost 90%. The camera exposure time was set to 10 ms.

The two tested sCMOS cameras were a Kinetix 22 (Teledyne Photometrics [13]) and a pco.edge 4.2bi (Excelitas PCO [14]). Both have a wavelength-dependent quantum efficiency comparable to that of the EMCCD. A particularity of the Kinetix 22 are its four different acquisition modes, which differ in bit depth, read noise, line time and camera gain. Most measurements for the Kinetix 22 were performed in the so called Sub-Electron Mode, in which two rows are sampled simultaneously, and the intensity of each pixel is digitized eight times [15].

Since these sCMOS cameras have a rolling shutter readout, special care has to be taken to illuminate all lines simultaneously during the LED's light pulse. To this end, the exposure time was set to 34 ms for the pco.edge 4.2bi and to 10 ms for the Kinetix 22 in the Sub-Electron Mode.

The ICCD consists of a BV 2581 TX-V 100N Image Intensifier (custom design by Proxivision, now part of company Exosens [16]) containing an S20 UV-enhanced photocathode, a variable gain double MCP, a P46 phosphor screen and a relay lens for imaging the screen to a C-mount camera of choice. In our case, this was a standard machine-vision CMOS camera (Basler ace acA1920-40gm). Due to the high gain operation of the MCP, single photons lead to bright spots on the phosphor screen. The photo-cathode quantum efficiency achieves about 15 % at a wavelength of ≃ 450 nm.

DARK COUNT MEASUREMENTS

Dark count measurements were performed with the EMCCD, the ICCD and the pco.edge 4.2bi camera. Increasing the exposure time of the EMCCD and sCMOS cameras cause a non-linear increase of the mean gray values, see Fig. 2. For the sCMOS camera, a sensor-internal low dc mode activated for exposure times larger than 60 ms may cause this non-linearity. The mean gray values are determined in a square containing 750x750 pixels and 32 frames, respectively. The error bars correspond to one standard deviation between the individual images.

For the ICCD, the number of dark counts increases linearly with the exposure time, see Fig. 3 and depends on the MCP gain. For an MCP gain control voltage of 4.5 V (range 0 to 5 V) the dark electron emission rate of the photo-cathode was determined to be (452 ± 64) electrons/cm^2/s. An exposure time of 10 ms and an MCP gain of 2.5 V result in a neglectable number of intensifier dark counts as compared to the signal with lowest fluence used for the characterization of all cameras (duration 0.5 ms). Therefore, for the results presented hereafter, only the CMOS background has been subtracted.

For the EMCCD and sCMOS cameras, background reference images generated by averaging 32 frames and applying a median filter with a radius of 2 pixels, were subtracted.

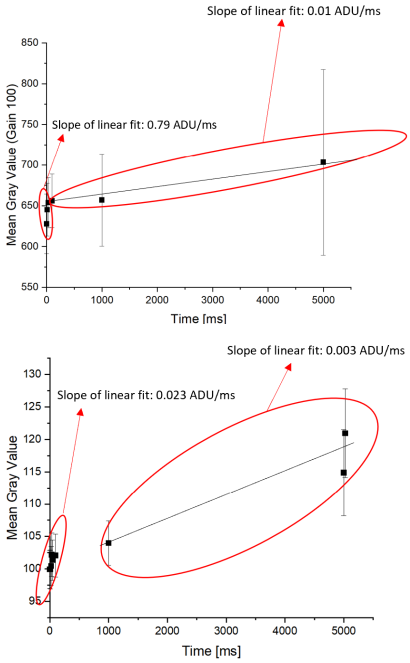

Figure 2: Mean gray values (dark counts) as a function of exposure time for the EMCCD at gain 100 (top) and for the pco.edge 4.2bi (bottom).

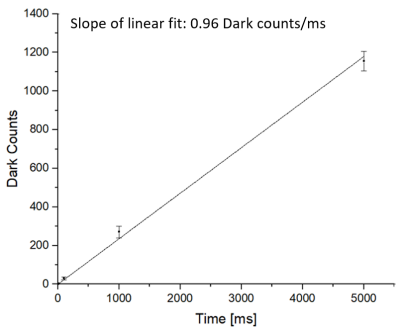

Figure 3: Dark counts as a function of exposure time for an MCP Gain of 4.5 V for the ICCD.

PROJECTIONS OF A ROI

The horizontal and vertical projections of a region of interest (ROI) containing the PTFE pattern were investigated for different light pulse durations and wavelengths. The vertical projection is considerably stronger affected by the inhomogeneous illumination of the ROI, hardly avoidable with the present set-up. Exemplarily, images of the ROI for a light pulse of 0.5 ms at 500 nm are shown in Figs. 4 and 5 as acquired with the EMCCD at gain 100 and the pco.edge 4.2bi.

At light pulse duration shorter than 0.5 ms images from the EMCCD and sCMOS cameras start getting very faint, and the ROI projection significantly degrade. ICCD images, however, provide for ROI projections of acceptable quality even with 0.05 ms pulses, see Fig. 6. This figure also shows that the ICCD is sensitive to reflections at the blackened aluminium foil on which the PTFE pattern is applied.

ISBN: 978-3-95450-249-3 ISSN: 2673-5350 doi: 10.18429/JACoW-IBIC2024-WEP30

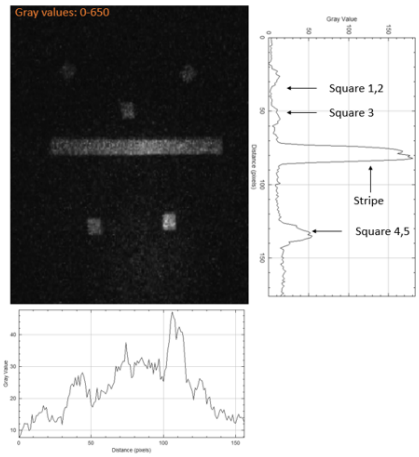

Figure 4: ROI image and its horizontal (right) and vertical (below) projections as acquired with the EMCCD at gain 100. Light pulse: 0.5 ms at 500 nm.

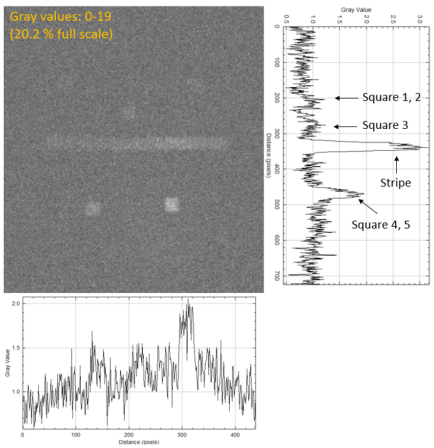

Figure 5: ROI image and its horizontal (right) and vertical (below) projections as acquired with the pco.edge 4.2bi. Light pulse: 0.5 ms at 500 nm.

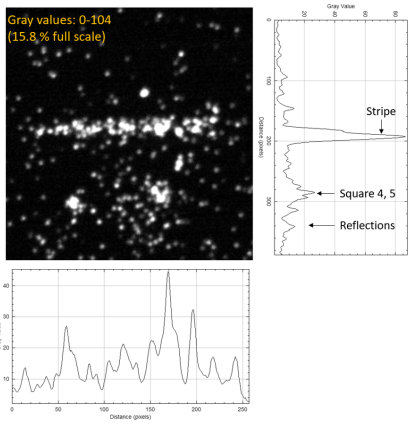

Figure 6: ROI image and its horizontal (right) and vertical (below) projections as acquired with the ICCD. Light pulse: 0.05 ms at 500 nm.

The ratio of the mean top intensity of the horizontal projection of the stripe's image to the standard deviation σ of the intensity determined in a "dark" ROI away from the PTFE pattern is shown in Fig. 7 as function of different light pulse duration.

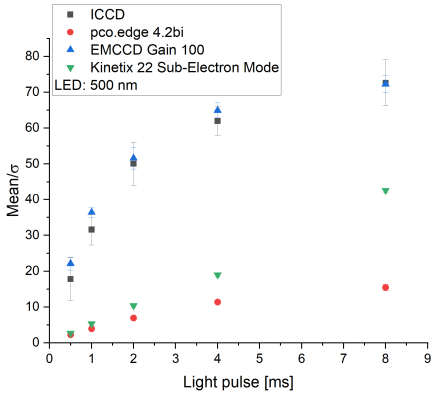

Figure 7: Mean to σ ratios for different light pulses at 500 nm.

SIGNAL-TO-NOISE RATIO

Due to the LEDs' relatively narrow emitting angle, the pattern is illuminated inhomogeneously. Hence, for each LED, a small ROI on the pattern's stripe was defined, over which the illumination was homogeneous to a good approximation. Within this ROI, the average number of photons per square millimeter was estimated using single-photon counting with the ICCD and confirmed with the EMCCD and sCMOS cameras. The results are collected in Table 1.

Table 1: Average Number of Photons per Square Millimeter Sensor Area for Different Wavelengths and 0.5 ms Pulses

Wavelength [nm]	Photons/mm^2
500	$(54 \pm 9) \times 10^3$
470	$(32 \pm 5) \times 10^3$
385	$(39 \pm 14) \times 10^3$

A comparison of the Signal-to-noise ratios (SNR) at 500 nm as function of pulse duration is given in Fig. 8 for all cameras and all Kinetix 22 tested modes. The SNR of the two sCMOS cameras are not far apart, but the range over which they extend grows with the exposure time by a factor of approximately 4. An influence on the SNR is detectable for the Kinetix 22 different modes; e.g., the Sub-Electron Mode is about a factor 1.4 more sensitive than the Dynamic Range Mode. For the pco.edge 4.2bi the SNR is in between the Kinetix 22 acquisition modes. The SNR of the ICCD is slightly higher than the best SNR of the sCMOS cameras, i.e. those of the Kinetix 22 Sub-Electron Mode. Finally, the SNR of the EMCCD at gain 100 are distinctly higher than the others.

For a shorter wavelength of 470 nm, as shown in Fig. 9, the sensitivity of the EMCCD and the ICCD levels off. It is related to the larger quantum efficiency of the ICCD, while

ISBN: 978-3-95450-249-3 ISSN: 2673-5350 doi: 10.18429/JACoW-IBIC2024-WEP30

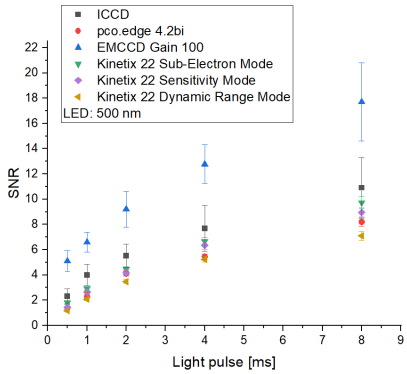

Figure 8: SNR as a function of light pulse duration for all cameras and Kinetix 22 tested modes at 500 nm.

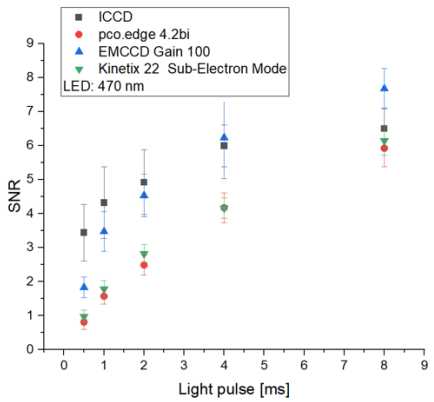

Figure 9: SNR as a function of light pulse duration for all cameras (Kinetix 22 in Sub-Electron Mode) at 470 nm.

the other solid-state sensor-based cameras have an SNR similar to that at a wavelength of 500 nm.

At 385 nm, however, the ICCD SNR is noticeably better than for any other tested camera, see Fig. 10. Besides, for a pulse duration of 8 ms, the ROI at the ICCD got overexposed; hence, an SNR value is not depicted. Even for 4 ms, a few pixels in the ROI were overexposed. The SNR of the Kinetix 22 in Sub-Electron Mode is somewhat lower than at 500 nm

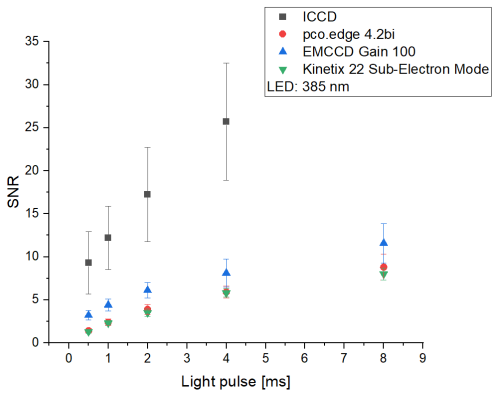

Figure 10: SNR as a function of light pulse duration for all cameras (Kinetix 22 in Sub-Electron Mode) at 385 nm.

and basically equal to those of the pco.edge 4.2bi, while those of the EMCCD at gain 100 are perceptibly higher.

SPATIAL RESOLUTION

The resolution at the sensor plane was determined with a USAF 1951x resolution target (Target USAF 3" x 3" NEG, Edmund Optics) placed in the dark enclosure at (88.8 ± 0.2) cm from the objective lens. The negative test chart was illuminated from behind with a luminescent foil. For calculating the resolution at the sensor plane of the EMCCD and sCMOS cameras, the image scale of the objective lens (0.0181 ± 0.0001) was considered. For the ICCD, the image scale of the relay lens (0.589 ± 0.015) had to be considered too. The sCMOS cameras have the best resolution with 55.2 lp/mm, while the EMCCD achieves 31.1 and the ICCD 23.5 lp/mm.

CONCLUSION

A set-up for low-light camera characterization has been built. The pulsed LEDs used as light source (nominal wavelengths from 385 to 500 nm, and pulse duration from 0.05 ms to 8 ms) were characterized.

The sCMOS cameras have the best spatial resolution at the sensor plane compared to the EMCCD and the ICCD.

The ICCD is the most sensitive camera as a light pulse of 0.05 ms was sufficient to generate an acceptable horizontal projection of the ROI. This was not possible with any of the other tested cameras, which needed an order of magnitude larger pulse lengths for comparable results. Due to the single-photon capability, the ICCD can lead to an absolute fluence determination.

Signal-to-noise ratios within a homogeneously illuminated ROI were determined. The ICCD delivers the best results at short wavelengths. This is related to the photocathode's quantum efficiency ranging to near UV. For visible light at longer wavelengths, the EMCCD offers the same or even higher SNR due to the solid-state sensor's quantum efficiency with a peak at about 600 nm.

Both sCMOS cameras have about a factor of 7 lower sensitivity than the EMCCD. While using the sCMOS cameras, the rolling shutter readout, especially the readout time needed for one line, had to be considered to correctly acquire the entire light pulse. Further results with different SNR characterizations are discussed in [11]. Even though different cameras have been investigated, the general tendency coincides with the results described in [10].

ACKNOWLEDGMENTS

The authors thank Christiane Andre, Rainer Haseitl, Piotr Kowina, Beata Walasek-Höhne, and Tobias Luckhardt (GSI); Ulrich Ratzinger, and Hendrik Hähnel (Goethe-Universität); Walther Tutsch (Excelitas PCO), and Mathias Pasche-Drews (Teledyne) for their support.

ISBN: 978-3-95450-249-3 ISSN: 2673-5350 doi: 10.18429/JACoW-IBIC2024-WEP30

REFERENCES

[1] C. A. Andre *et al.*, "Beam Induced Fluorescence (BIF) Monitors as a Standard Operating Tool", in *Proc. DIPAC'11*, Hamburg, Germany, May 2011, paper MOPD60, pp. 185–187.

[2] C. Andre, P. Forck, R. Haseitl, A. Reiter, R. Singh, and B. Walasek-Hoehne, "Optimization of Beam Induced Fluorescence Monitors for Profile Measurements of High Current Heavy Ion Beams at GSI", in *Proc. IBIC'14*, Monterey, CA, USA, Sep. 2014, paper TUPD05, pp. 412–416.

[3] O. Sedlacek *et al.*, "Gas Jet-Based Fluorescence Profile Monitor for Low Energy Electrons and High Energy Protons at LHC", in *Proc. IBIC'23*, Saskatoon, Canada, Sep. 2023, pp. 312–317. doi:10.18429/JACoW-IBIC2023-WE3I01

[4] H. Zhang *et al.*, "BGC monitor: First year of operation at the LHC", presented at IBIC'24, Beijing, China, Sep. 2024, paper FRAC2, this conference.

[5] C. Bal, E. Bravin, E. Chevallay, T. Lefevre, and G. Suberlucq Geneva, "OTR from Non-Relativistic Electrons", in *Proc. DIPAC'03*, Mainz, Germany, May 2003, paper PM04, pp. 95–97.

[6] O. Sedlacek *et al.*, "Optical transition radiation measurements of a high intensity low energy hollow electron beam on electron beam test facility", in *Proc. IPAC'23*, Venice, Italy, May 2023, pp. 3952–3955. doi:10.18429/JACoW-IPAC2023-THPA002

[7] R. Singh, T. Reichert, and B. Walasek-Hoehne "Optical transition radiation based transverse beam diagnostics for non-relativistic ion beams", *Phys. Rev. Accel. Beams*, vol. 25, p. 072801, Jul. 2022. doi:10.1103/PhysRevAccelBeams.25.072801

[8] F. Becker, F. M. Bieniosek, P. Forck, D. H. H. Hoffmann, and P. N. Ni, "Beam Induced Fluorescence (BIF) Monitor for Intense Heavy Ion Beams", in *Proc. BIW'08*, Lake Tahoe, CA, USA, May 2008, paper TUPTPF054, pp. 236–240.

[9] P. Forck, C. A. Andre, F. Becker, R. Haseitl, and B. Walasek-Hoehne, "Beam Induced Fluorescence Profile Monitor Developments", in *Proc. HB'10*, Morschach, Switzerland, Sep.-Oct. 2010, paper WEO1C03, pp. 497–501.

[10] R. Hampf, A. Ulrich, and J. Wieser, "Evaluation of CCD cameras for beam profile monitoring with high intensity particle beams traversing gases", *EPJ Tech. Instrum.*, vol. 7, no. 5, 2020. doi:10.1140/epjti/s40485-020-00057-0

[11] Leonie Bauer, "Characterization of low-light Cameras for Beam Diagnostics", Master thesis, Goethe-Universität, Frankfurt, Germany, 2024. Thesis can be found on https://publikationen.ub.uni-frankfurt.de/solrsearch/index/advanced

[12] www.princetoninstruments.com/products/proem-family/pro-em

[13] www.photometrics.com/products/kinetix-family/kinetix22

[14] www.excelitas.com/de/product/pcoedge-42-bi-usb-scmos-camera

[15] Teledyne Photometrics, *Kinetix Manual*, 58-723-004 Rev A01, 2021.

[16] www.exosens.com/company-about-exosens/photonis-germany-gmbh